RESEARCH ARTICLE SUMMARY

CHEMISTRY AUTOMATION

Automated self-optimization, intensification, and scale-up of photocatalysis in flow

Aidan Slattery†, Zhenghui Wen†, Pauline Tenblad†, Jesús Sanjosé-Orduna, Diego Pintossi, Tim den Hartog, Timothy Noël*

INTRODUCTION: Photocatalysis exploits light for driving reactivity under mild conditions, contributing to advancements in synthetic methods for pharmaceuticals, agrochemicals, and materials. Nonetheless, challenges persist in optimizing, replicating, and scaling these techniques. These challenges stem from practical considerations such as uneven light absorption and experimental variability, alongside chemical complexities such as poorly understood reaction mechanisms and intricate interactions among various variables. These phases in advancing photocatalytic processes are crucial yet time-consuming components of contemporary chemical manufacturing, requiring expertise and precision owing to their intricate and sensitive nature.

RATIONALE: In response to the need for efficient optimization of complex photocatalytic reaction conditions, we have developed a robotic platform named RoboChem. RoboChem facilitates the self-optimization, intensification, and scale-up of photocatalytic transformations. By integrating readily available hardware, customized software, and a Bayesian optimization (BO) algorithm, this platform offers a hands-free and safe solution, mitigating associated challenges. Operating autonomously, RoboChem eliminates the requirement for extensive expertise in photocatalysis or scaling processes to achieve optimal results. This renders RoboChem a valuable collaborative robotic platform suitable for any synthetic organic chemistry laboratory, irrespective of users' specific familiarity with photocatalysis.

RESULTS: The robotic platform incorporates several key components, including a liquid handler, syringe pumps, a tunable continuous-flow photoreactor, cost-effective Internet of Things devices, and an in-line nuclear magnetic resonance (NMR) system. It uses a closed-loop BO approach to systematically explore a chosen parameter space encompassing both discrete and continuous variables. Consequently, the platform excels in identifying optimal reaction conditions that maximize either yield, throughput, or a combination thereof.

Operating within a continuous flow microreactor, the platform effectively addresses mass, heat, and photon transport considerations, resulting in the generation of well-structured datasets. These datasets capture both positive and negative results, thereby highlighting the influence of specific variables on the targeted objective function.

Furthermore, the optimal conditions identified by the platform have been successfully scaled up within the same continuous flow photoreactor. Manual isolation processes have been applied to obtain meaningful quantities of pure isolated compounds. Notably, the isolated yields closely align with the NMR yields obtained by the platform, validating its high precision and reliability.

The platform's capabilities were demonstrated across a diverse set of 19 molecules, covering various facets of photocatalysis, such as hydrogen atom transfer photocatalysis, photoredox catalysis, and metallaphotocatalysis. Notably, human involvement was limited to the definition of the parametric space, the preparation of stock solutions and the isolation of pure compounds. The effectiveness of the platform stems from its BO algorithm, which efficiently captures intricate interdependencies among different reaction variables. Consequently, the platform consistently identified optimal reaction conditions that either matched or exceeded those obtained through manual approaches. As a result, the RoboChem platform stands out from conventional synthetic methods by tailoring reaction conditions to the specific needs of each substrate. This capability enables a thorough assessment of the applicability and limitations of the reported transformations, ultimately enhancing their value for potential industrial implementation.

CONCLUSION: The RoboChem robotic platform expedites and streamlines the optimization of photocatalytic transformations, simultaneously enhancing safety and liberating researchers to focus on other creative facets of chemistry. ■

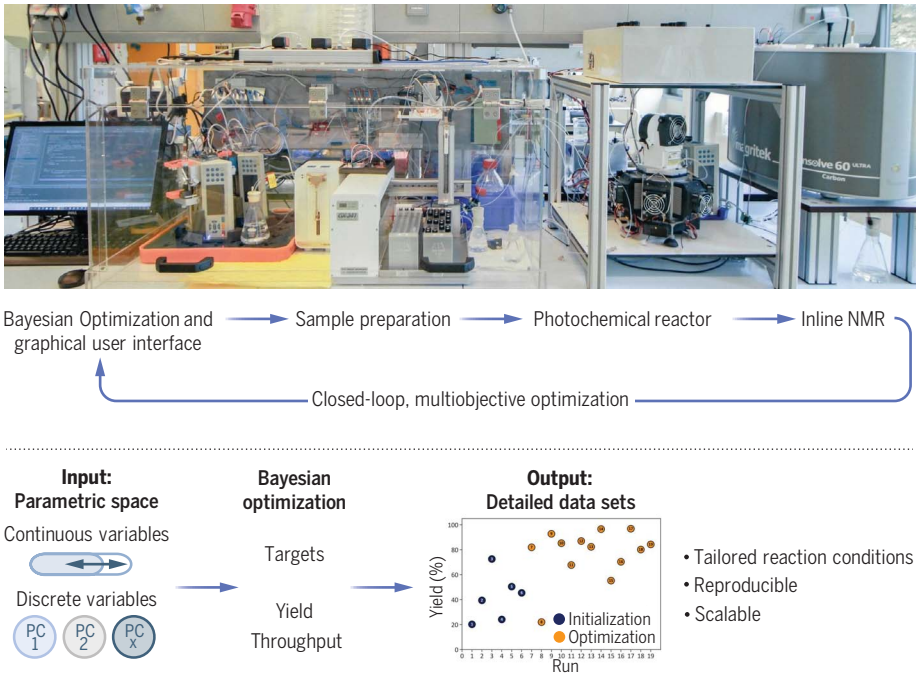

RoboChem: a benchtop robotic platform for the self-optimization, intensification and scale-up of photocatalytic transformations.

The list of author affiliations is available in the full article online.
*Corresponding author. Email: t.noel@uva.nl
†These authors contributed equally.
Cite this article as A. Slattery *et al.*, *Science* **383**, eadj1817 (2024). DOI: 10.1126/science.adj1817

READ THE FULL ARTICLE AT
https://doi.org/10.1126/science.adj1817

RESEARCH ARTICLE

CHEMISTRY AUTOMATION

Automated self-optimization, intensification, and scale-up of photocatalysis in flow

Aidan Slattery[1]†, Zhenghui Wen[1]†, Pauline Tenblad[1]†, Jesús Sanjosé-Orduna[1], Diego Pintossi[1], Tim den Hartog[1,2,3], Timothy Noël[1]*

The optimization, intensification, and scale-up of photochemical processes constitute a particular challenge in a manufacturing environment geared primarily toward thermal chemistry. In this work, we present a versatile flow-based robotic platform to address these challenges through the integration of readily available hardware and custom software. Our open-source platform combines a liquid handler, syringe pumps, a tunable continuous-flow photoreactor, inexpensive Internet of Things devices, and an in-line benchtop nuclear magnetic resonance spectrometer to enable automated, data-rich optimization with a closed-loop Bayesian optimization strategy. A user-friendly graphical interface allows chemists without programming or machine learning expertise to easily monitor, analyze, and improve photocatalytic reactions with respect to both continuous and discrete variables. The system's effectiveness was demonstrated by increasing overall reaction yields and improving space-time yields compared with those of previously reported processes.

Photocatalysis has greatly advanced synthetic methods by leveraging a range of distinct mechanistic pathways, such as single electron transfer, energy transfer, and hydrogen atom transfer (HAT) (*1*). Its inherently mild nature allows for seamless integration with other catalytic processes, facilitating distinct transformations achievable only through the synergistic action of multiple catalysts (*2*). Despite these advancements, the field still grapples with substantial hurdles in optimization, replication, and scalability of these methods (Fig. 1) (*3*).

These difficulties partly arise from the chemical complexity of photocatalysis, involving poorly understood reaction mechanisms and limited understanding of the photophysics underpinning the observed reactivity (*4*). Additionally, the complex synergistic interactions between different reaction variables often go unnoticed in traditional academic optimization strategies (*5*). When a promising reaction is initially identified, the focus shifts to refining conditions for that specific substrate by using the "one-factor-at-a-time" (OFAT) method. This approach entails systematically adjusting individual variables, such as ligands, bases, solvents, or in rare cases, light intensity, retaining the best result before proceeding to the next. Although design-of-experiments (DoE) strategies are increasingly adopted in industrial settings, applying them to each substrate within a scope is resource intensive. To save time, conditions optimized for a benchmark substrate are often generically applied to others, leading to suboptimal yields or selectivity. This is because each substrate has distinct molecular characteristics, such as differing steric and electronic properties and the presence or absence of sensitive functional groups, all of which substantially influence the reaction's outcome.

Another challenge in developing photocatalytic methods lies in the variability of experimental setups, leading to substantial batch-to-batch inconsistencies and limited scalability (*6*). In photocatalysis, photons act as central reactants, meaning that the reaction rate and stability of reagents closely depend on light intensity. According to the Lambert-Beer law, light intensity diminishes rapidly as it travels through a photocatalytic reaction mixture. Therefore, traditional batch scale-up strategies, which simply enlarge reactor dimensions, are ineffective, as major portions of the reactor receive insufficient light. Furthermore, uneven light distribution can cause irreproducibility, extended reaction times, and unwanted byproduct formation. Flow reactors, integrated with high-power light sources, have thus become crucial for effectively scaling up photocatalytic transformations, even in industrial settings (*7*, *8*). These reactors guarantee uniform high light intensity across the entire reactor cross-section, enhancing reaction kinetics and reducing reaction times, a concept known as process intensification (*9*). However, variations in light sources and reactor geometry mean that even with flow reactor technology, reoptimization is often necessary to ensure compatibility with the specific photocatalytic transformation.

In response to the challenge of rapidly optimizing complex photocatalytic reaction conditions, we sought to develop a multipurpose robotic platform, called RoboChem, that enables the self-optimization, intensification, and scale-up of photocatalytic transformations (Fig. 1). This platform overcomes associated challenges by integrating off-the-shelf hardware and customized software, providing a hands-off solution. Our open-source platform combines a liquid handler, syringe pumps, a high-powered photoreactor, inexpensive Internet of Things (IoT) devices, and an in-line benchtop nuclear magnetic resonance (NMR) system to enable automated and data-rich optimization. By using a continuous-flow capillary photoreactor, our platform ensures highly reproducible data collection, effectively mitigating issues related to mass, heat, and photon transport that often contribute to irreproducibility in photocatalytic transformations (*10*, *11*).

Further, to account for complex intercorrelations between reaction variables, optimization algorithms such as DoE and statistical modeling can be integrated into the platform. However, for complex nonlinear relationships such as those encountered in photocatalytic reactions, machine learning proves to be a more effective approach (*12*). Its capacity to rapidly and efficiently analyze vast amounts of data enables the identification of underlying patterns and the extraction of meaningful conclusions (*13*). Thus, combining machine learning with reaction automation is advantageous (*14*). Given that our platform operates as a linear system (i.e., not parallelized), minimizing the number of experiments required to reach optimal conditions was crucial. For this reason, we turned to Bayesian optimization (BO), which has gained popularity in the chemistry community owing to its capacity to optimize black-box functions (*15*–*17*).

As an automated flow chemistry setup, our platform is capable of exploring large regions of the experimental and chemical space within a relatively short period, making it well suited to address complex optimization problems encountered in photocatalytic reaction scope elaboration. The RoboChem platform distinguishes itself from common synthetic method practices by tailoring the reaction conditions to the specific requirements of every substrate, thereby enabling a clear evaluation of the applicability and limitations of the reported transformations, resulting in increased value for industrial implementation.

Because the capillary photoreactor is equipped with high-power LEDs, of which the light intensity can be adjusted to meet specific photochemical needs, this setup enables the production of

[1]Flow Chemistry Group, van 't Hoff Institute for Molecular Sciences (HIMS), University of Amsterdam, Science Park 904, 1098 XH Amsterdam, Netherlands. [2]Zuyd University of Applied Sciences, Nieuw Eyckholt 300, 6419 DJ Heerlen, Netherlands. [3]Netherlands Organisation for Applied Scientific Research (TNO), High Tech Campus 25, 5656 AE Eindhoven, Netherlands.
*Corresponding author. Email: t.noel@uva.nl
†These authors contributed equally.

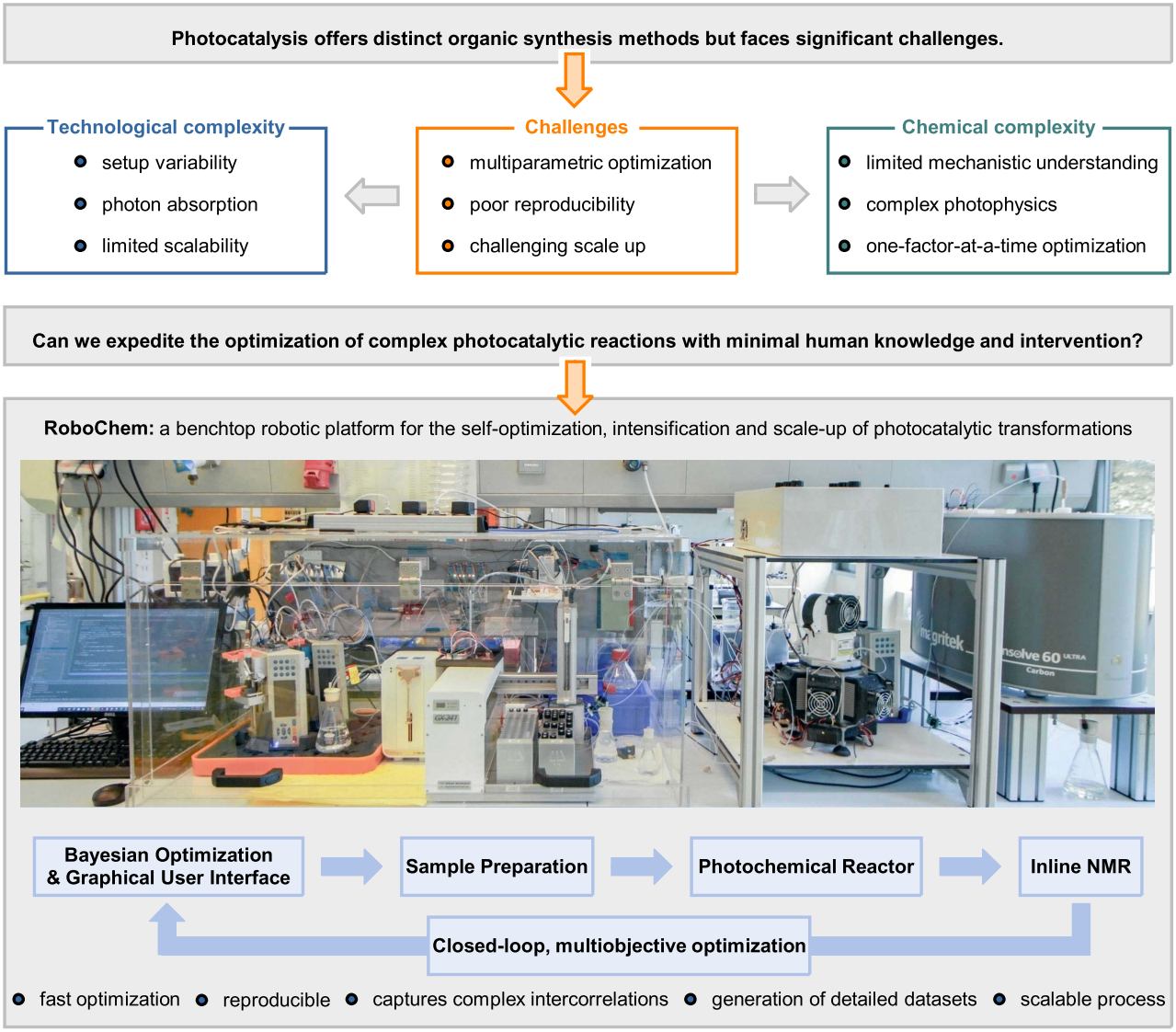

Fig. 1. RoboChem: a benchtop platform for the closed-loop, multiobjective optimization of photocatalytic systems. Shown are the challenges associated with optimization, replication, and scalability of photocatalysis, as well as the robotic platform and its workflow.

materials in substantial quantities. Consequently, results obtained from small-scale experiments can be seamlessly scaled up in the same reactor to produce tens to hundreds of grams of material per day, bridging the gap between laboratory research and practical application. Operating entirely autonomously, the platform further eliminates the need for in-depth expertise in photocatalysis or scaling processes to achieve optimal outcomes. This makes RoboChem an effective collaborative robotic platform, suitable for use in any synthetic organic chemistry laboratory, regardless of the users' specific knowledge in photocatalysis. In this work, we demonstrate the general applicability of RoboChem to the optimization of a diverse set of photocatalytic transformations, including hydrogen atom transfer (HAT) photocatalysis, photoredox catalysis, and metallaphotocatalysis, which are relevant to medicinal and crop protection chemistry.

RoboChem platform

The RoboChem platform can be divided into three distinct workflows: the controller, the planner, and the user input (Fig. 2A). The hardware controller guides the physical platform, encompassing tasks such as preparing the reaction mixture, executing the experiment, and conducting subsequent in-line analysis. The planner, which is a machine learning model, is responsible for determining the optimal experiments to run by selecting parameters and communicating them to the controller. The results are then fed back to the machine learning model, which subsequently recommends the next experiment. Last, the graphical user interface (GUI) allows users to input the necessary parameters, launch the optimization campaign, and initiate the process.

Platform – Controller

RoboChem is controlled by custom Python code and uses open-source libraries (Fig. 2A) with off-the-shelf instruments and devices. By coupling a liquid handler, syringe pumps, switching valves, a high-power continuous-flow photoreactor, as well as simple IoT devices such as phase sensors and ultrasonic detectors with an in-line 60-MHz benchtop NMR spectrometer for data-rich optimization, we have come up with a workflow to easily and efficiently optimize and intensify

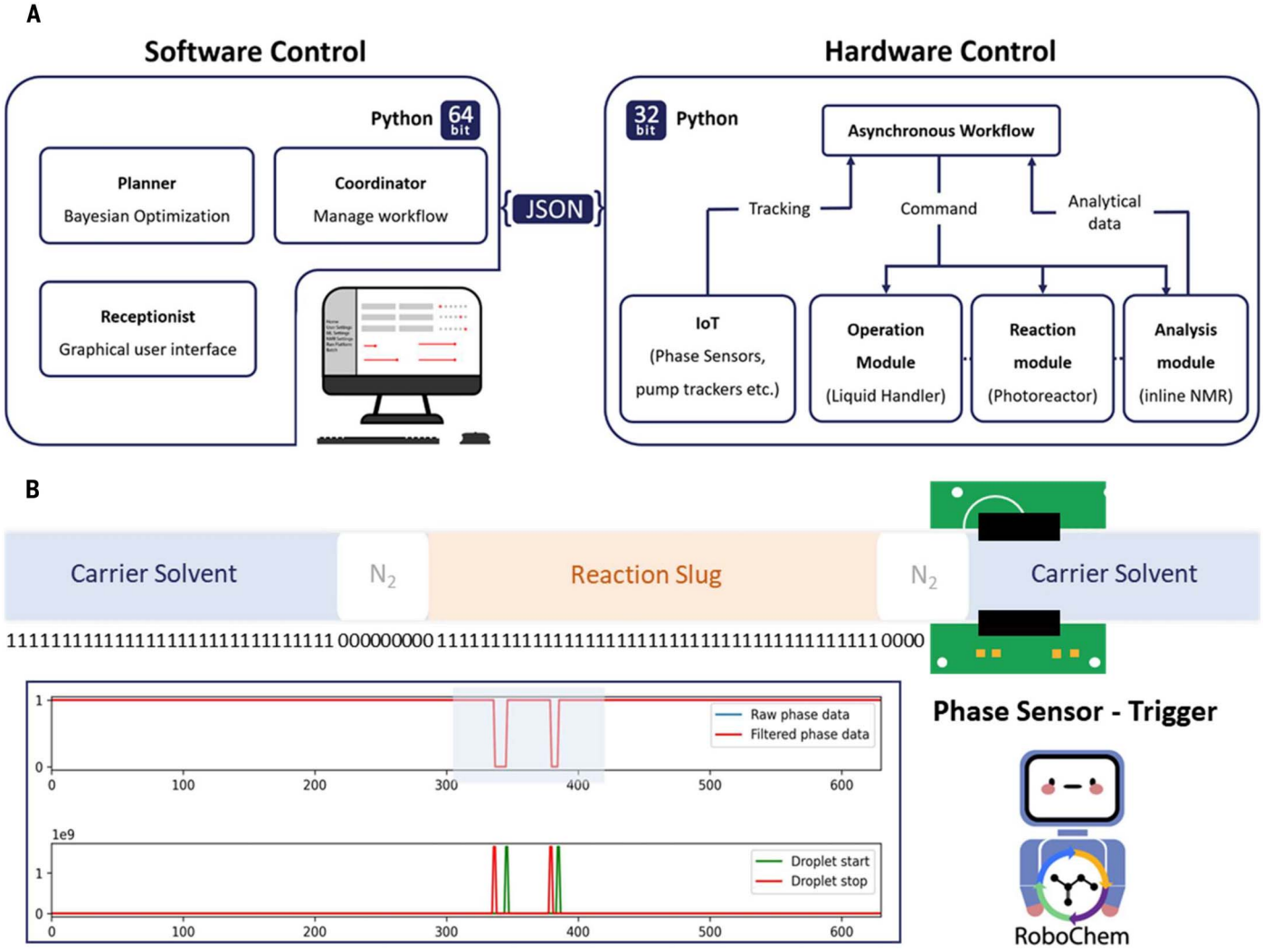

Fig. 2. Automated robotic platform for the self-optimization, intensification, and scale-up of photochemistry in flow. (**A**) High-level view of platform architecture. (**B**) Reaction tracking on the platform carried out by phase sensors to allow for timely triggering of events. A reaction slug is tracked as it passes over a phase sensor and investigated by an algorithm to form a trigger for the next phase of the optimization cycle.

photochemical processes. Each generated reaction slug (650 μL) represents a discrete set of reaction conditions (*18*, *19*), and the reactions are executed sequentially: sample preparation, reaction under the specified conditions, and automated analysis and processing. We used NMR for data analysis, which accurately integrates yields without requiring prior calibration of the analytics by using an analytically pure sample. This approach enabled us to conduct most reactions without the need for an internal standard, opting instead for an externally calibrated standard with a peak in a similar parts-per-million range as the target molecule. Although a 60-MHz benchtop NMR spectrometer was selected as the analytical technique, the platform is easily adaptable to accommodate other analytical techniques, such as Raman spectroscopy, infared spectroscopy, high-performance liquid chromatography (HPLC)–ultraviolet (UV) visible light, HPLC–mass spectrometry (MS), or gas chromatography–MS. Because the volume of the reaction slug is determined by the analytical method, this parameter could be substantially reduced by an order of magnitude if an alternative technique like HPLC were to be used. (*20*)

The RoboChem platform operates in a closed-loop manner, driven by the BO algorithm. This iterative process involves the BO algorithm proposing experiments, which are automatically executed and analyzed. The obtained results are then fed back into the BO algorithm, which generates a new set of conditions for further optimization (*21*, *22*). By harnessing the capabilities of a photomicroreactor equipped with high-intensity LEDs (*23*) and the ability to make computer-controlled power output adjustments, we can minimize reaction times and substantially enhance the throughput of the platform. This increased efficiency reduces the time required for a comprehensive optimization run.

By using a series of phase sensors and a dedicated algorithm to detect the passage of a reaction slug (*24*), the platform can efficiently track its position (Fig. 2B). This cost-effective approach enables precise control over the reaction as it traverses the system. The ability to accurately monitor the reaction's location eliminates the need to hardcode pump volumes, allowing for seamless compatibility with reactors of varying sizes without requiring any code modifications. Moreover, this tracking capability facilitates precise "parking" of the reaction slug in the NMR system for analysis, optimizing reagent usage by minimizing the required quantity for each reaction condition.

The entire system is conveniently located on a standard laboratory benchtop and is enclosed within a custom-designed, closed suction box, eliminating the need for placement within a fume hood during reaction runs. The system's design facilitates three distinct operating modes:

(i) Single experiment: Conducting a reaction under specific conditions, whether for the purpose of yield or productivity discovery, or as part of a scope entry.

(ii) Self optimization: Automating the optimization process for a single reaction or multiple reactions consecutively.

(iii) Scale-up: Exploiting the optimized conditions obtained through self-optimization for efficient scaling up of the reaction.

Bayesian optimization – Planner

The platform leverages BO, a machine learning–based approach, to optimize chemical reactions. BO is a probabilistic model-based method designed to efficiently identify the maximum (or minimum) of an unknown black-box function (*25*). It constructs a probability model of the function using carefully selected samples, which guides the search process by suggesting the next point to evaluate. The BO model incorporates both exploitation and exploration strategies. Exploitation involves investigating areas predicted to have the highest value, whereas exploration focuses on exploring points where the model has limited knowledge. This dual approach prevents the model from becoming trapped in local maxima or minima. The iterative process continues with the model being updated after each new evaluation of the function until a predetermined threshold is reached or a specific number of experiments have been conducted.

The BO model was implemented with the open-source Python package Dragonfly, developed by Kandasamy and collaborators (*22*, *26*). The initial runs are chosen by using Latin-hypercube sampling (*27*, *28*). The researchers define the input variables (parameters to be tuned) and the objective to be optimized. The platform supports both single-objective and multiobjective optimization, targeting yield and/or throughput. In single-objective optimization, the model identifies the global maximum of the reaction. In multiobjective optimization, the model finds a set of nondominated solutions known as the Pareto front (*29*). To assess the progress of the optimization problem, the platform tracks the hypervolume after each run (*30*). In cases of interrupted runs or the desire to build upon previously executed experiments, the platform allows for further optimization from that point (for further details, see the supplementary materials).

The platform's integration of machine learning effectively reduces the reliance on human resources (*31*, *32*). Once the experiments are set up and the optimization process is initiated, the platform operates independently. The machine learning model autonomously determines the next set of experiments to run, and the corresponding commands are automatically transmitted to the platform. As a result, the platform can run continuously, including overnight, freeing up the chemist to focus on other tasks. Throughout this study, human intervention was mainly needed for replenishing solutions. Notably, we successfully prevented clogging issues by using a compact reaction slug that efficiently contained any minor precipitates. After this reaction phase, we maintained a continuous flow of a carrier solvent, such as acetonitrile or DMSO, to remove any remaining precipitates. It is important to note that while we did not encounter clogging in our experiments, the possibility of clogging cannot be ruled out if a flow-incompatible chemical space is chosen.

Graphical user interface – User input

A key aspect of the platform's design is the development of an intuitive graphical user interface (GUI) that enables chemists without programming or machine learning expertise to easily navigate the system. The GUI provides functionality for creating new experiments, storing all the settings and results for an optimization run. It also allows users to generate the required positional and sample data used by the platform and liquid handler to prepare reaction slugs.

The liquid handler can accommodate multiple stock solutions of the same type. As the platform consumes stock solutions, it automatically tracks the quantity used. When one stock solution is depleted, the platform seamlessly transitions to the next vial containing a remaining stock solution. The GUI defines the entire chemical space to be explored under the Machine Learning Settings page.

In the Run Platform tab, a button initiates the platform, and the GUI continuously tracks the results. For single-objective optimizations, the GUI presents a chart displaying the objective function (yield or throughput) against the number of runs. In multiobjective optimizations, it provides a plot of yield versus throughput and includes a graph tracking the hypervolume.

The GUI performs validations to ensure all necessary files and chemical spaces are properly defined before allowing the platform to run. If multiple reagents are added to a subcategory, the GUI automatically treats them as discrete variables for the optimization process.

After each run, the data consisting of both the input parameters and the output values are automatically stored in a JSON file. These JSONs have been converted to Microsoft Excel (.xlsx) files for easier data manipulation and are available on Zenodo as .xlsx files (*33*) and in the supplementary materials in table format, in line with the FAIR principles for scientific data archiving (*34*). These datasets have the potential to be used in future projects; the data are of high quality owing to the absence of mass, heat, and photon transport issues. Given that all experiments are conducted on the same platform (including scale-up), experimental error is significantly reduced, ensuring that NMR-based yield estimations closely align with those achieved after isolation on a 1- to 5-mmol scale. Another advantage is the accumulation of data for negative results, which are not commonly published but nevertheless are important for the development of machine learning models (*35*).

The primary focus of the RoboChem platform is to identify optimal reaction conditions for photocatalytic transformations. Our versatile platform caters to both single- and multiobjective optimization problems, offering synthetic chemists the ability to maximize yield, productivity, and other relevant objective functions. To accomplish this, we selected five distinct photocatalytic reactions, covering a total of 19 substrates, for optimization. For each case, we compared the yield and productivity reported in the literature with the conditions determined by the artificial intelligence (AI)–assisted RoboChem platform. The reaction conditions discovered by the AI were subsequently used to scale up the transformations.

Single-objective optimization for photocatalytic HAT alkylation

We began our testing and validation of the platform with a Giese-type reaction entailing photocatalytic HAT activation of hydrocarbons (*36*). The reaction was conducted in the flow photomicroreactor, using tunable 0- to 144-W, 365-nm–emitting light-emitting diodes (LEDs). This choice allowed us to evaluate robust and well-established chemistry in our laboratory (Fig. 3). Five optimization variables were selected for the reaction [benzylidenemalononitrile concentration, tetrahydrofuran (THF) loading, photocatalyst (TBADT) loading, light intensity, and residence time]. A total of 19 experiments were conducted in a closed-loop fashion continuously for 4 hours. The initiation phase involved six experiments, serving as a preliminary scan of the reaction space. Subsequently, the BO algorithm recommended one new experimental condition at a time for a further 13 experiments, aiming to maximize the objective function [yield (%)]. Within nine experiments, the platform achieved a yield of more than 90% and began converging on the optimal conditions for the chemistry, resulting in a yield exceeding 95% for the desired product. Notably, the reaction manifested a detrimental effect of high light intensity, with the optimal range found to be between 20 and 50% of full power (28 to 72 W

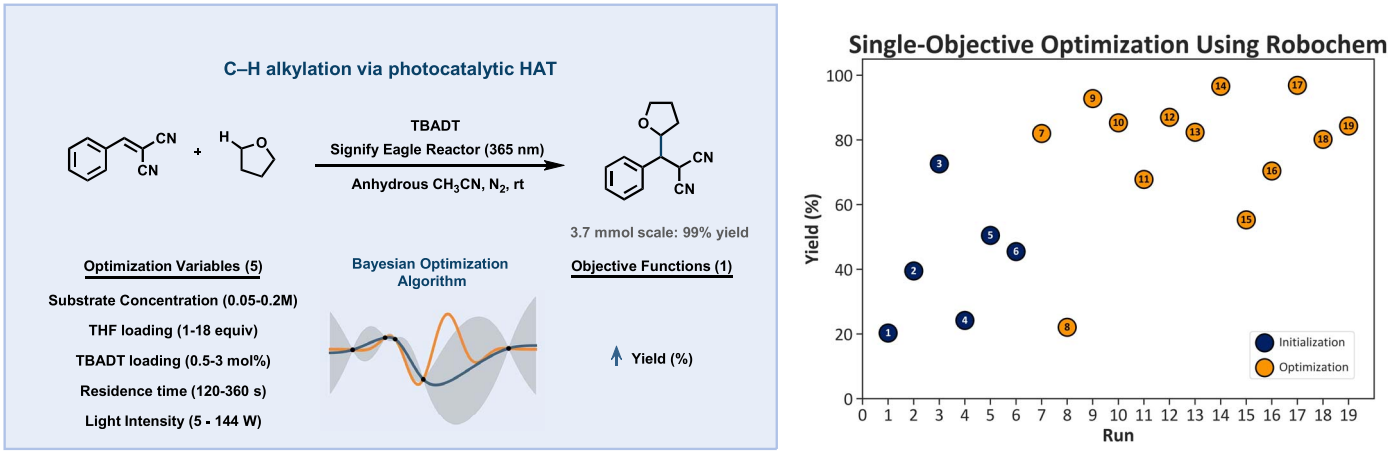

Fig. 3. Single-objective optimization of the photocatalytic HAT-alkylation of benzylidenemalononitrile with tetrahydrofuran (THF). rt, room temperature.

optical input power). These optimal conditions were then used for scaling up the transformation with the same capillary photoreactor, confirming the AI-determined yield with an isolated yield of 99% (3.7-mmol scale).

Single- and multiobjective optimization of C–H trifluoromethylthiolation of C(sp^3)–H and C(sp^2)–H bonds through decatungstate-enabled HAT

Having validated the automated AI-driven photochemical platform in a single objective optimization problem, we aimed next to investigate its capability for optimizing various photocatalytic processes in multiobjective fashion, seeking to simultaneously optimize yield and throughput. Consequently, the reaction conditions found by the AI model would be readily suitable for subsequent scale-up. As an initial benchmark, we selected the decatungstate-mediated trifluoromethylthiolation of C(sp^3)–H and C(sp^2)–H bonds through HAT, as reported in (*37*). The incorporation of the trifluoromethylthiol group in drug-like molecules holds high value in medicinal chemistry, offering high lipophilicity (as indicated by the Hansch parameter of π_R = 1.44) and electronegativity, which enhances the pharmacokinetic properties and optimizes the interaction between the active compound and its target.

In the trifluoromethylthiolation campaign (Fig. 4), five reaction parameters and two objective functions were optimized simultaneously. The photochemistry was conducted in the continuous-flow photomicroreactor, which used perfluoroalkoxy (PFA) tubing with a 0.8-mm I.D. and a total volume of 2.85 mL. To provide the necessary light source, a chip-on-board (COB) UV LED system with a tunable light intensity ranging from 0 to 144 W of optical power was used. The screening chemical space encompassed five continuous parameters: N-(trifluoromethylthio)phthalimide (Phth-SCF_3) concentration, H-donor equivalents, TBADT photocatalyst loading, residence time, and light intensity. The objective functions chosen for optimization were either yield (%) or simultaneously the yield (%) and throughput (mmol h^{-1}) of the SCF_3-bearing molecules. To ensure fair comparisons between different reactor systems, we chose to convert the productivities into space-time yield (STY) ($g{\cdot}L^{-1}{\cdot}h^{-1}$). This normalization factorizes the reactor volume, allowing for a more equitable assessment of performance across varying reactor sizes.

For each substrate, a total of 18 to 36 experiments were conducted within an 8- to 16-hour timeframe. This series comprised eight initialization experiments followed by refinement experiments for each optimization campaign until a sufficient yield or hypervolume was achieved. Notably, substantial yield improvements were observed compared with their respective model counterparts in batch reactions. The platform also demonstrated a remarkable increase in productivities, ranging from 70 to 100 times higher. Next, the reaction conditions selected by the AI model were successfully used for scale-up to 5 mmol. In all cases, the isolated yields obtained during the scale-up process closely matched the NMR yields observed with the AI-optimized reaction conditions.

Upon further analysis of the AI-discovered reaction conditions, several interesting observations emerged. The AI algorithm refined the reaction conditions to achieve optimal reactivity and selectivity for each specific substrate. In this context, the BO algorithm identified experimental conditions that deviated substantially from the standard conditions reported in (*37*). One notable finding was the substantial differences in reaction or residence time and light intensity, depending on the molecule being optimized. Comparing the results obtained for trifluoromethylthiolated Sclareolide (**5**) and Ambroxide (**6**), it is evident that the catalyst loading and light intensity are significantly lower for Ambroxide. This result can be rationalized by the fact that Ambroxide can undergo an additional reaction with another equivalent of Phth-SCF_3, resulting in a double-functionalized final product. However, such a reaction is not possible with Sclareolide, as the α-to-O carbon position is blocked by the carbonyl group. By reducing the catalyst loading and light intensity, the AI algorithm successfully enhanced the yield and selectivity of the monofunctionalized product (**6**).

Multiobjective optimization of oxytrifluoromethylation of alkenes by using photocatalytic single electron transfer

Next, we directed our focus to the oxytrifluoromethylation of alkenes through a three-component process using photocatalytic single electron transfer with $Ru(bpy)_3(PF_6)_2$, as reported by (*38*). In the oxytrifluoromethylation campaign (Fig. 5), we simultaneously optimized five reaction parameters: styrene concentration, CF_3 source loading, photocatalyst loading, residence time, and light intensity. Two objective functions [yield (%) and throughput (mmol h^{-1})] were targeted for optimization. Similarly, for each substrate, a total of 14 to 25 experiments were conducted within a 3- to 10-hour timeframe. The optimization process used rapid ^{19}F NMR analysis (2 min per measurement) for molecules **7**, **8**, **9**, and **11**. However, molecule **10** required a longer optimization time of 19 hours owing to the use of ^{1}H NMR for quantification. To ensure high accuracy, a 16-min analysis window was allocated per reaction. As previously described, our experimental procedure involved six initialization experiments, followed by refinement experiments for each optimization campaign.

Similar to previous experiments, the photochemistry was conducted in the flow photomicroreactor by using PFA tubing with a 0.8-mm I.D. However, for this campaign, chip-on-board blue LEDs with a tunable light intensity ranging from 0 to 188 W were manually installed to

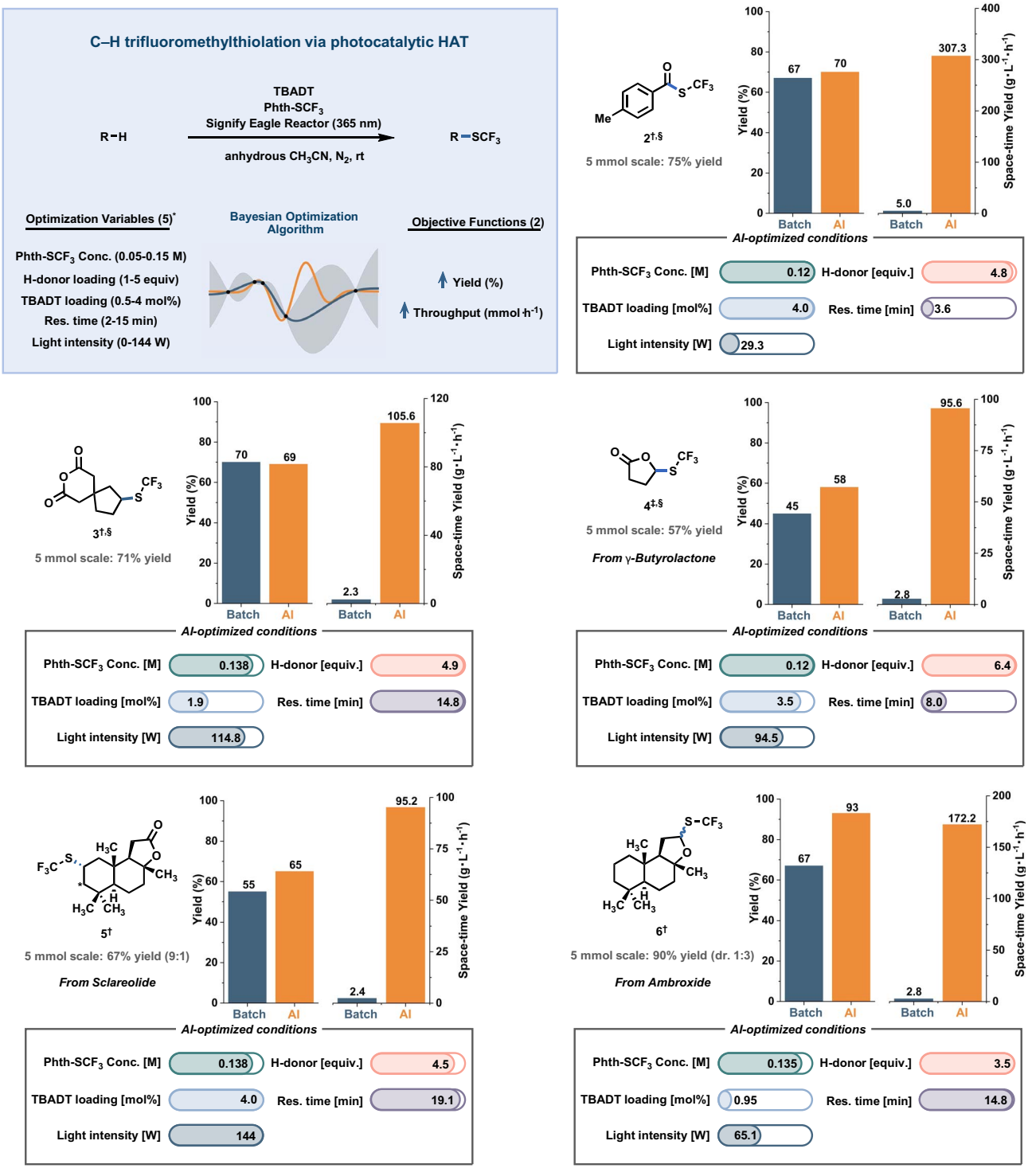

Fig. 4. Substrate scope and associated summary for the C–H trifluoromethylthiolation enabled by RoboChem. *Outer bounds of the chemical space explored for all experiments given (for more experimental details and exact chemical spaces explored for each experiment, see supplementary materials section S5.3). †Yield and space-time yield comparisons made directly from the literature. Conditions: PhthSCF_3 concentration (conc.) (0.2 M), H-donor equiv. [1.5 equiv. for aldehydes, 2.5 equiv. for substrates with activated C(sp^3)–H bonds, 5 equiv. for substrates with unactivated C(sp^3)–H bonds], TBADT loading (2.5 mol%), residence time (16 hours, 6 hours for aldehydes), light (385 nm, 1.2 W), N_2, 25°C. ‡Yield and space-time yield comparisons made to reactions carried out by us under literature conditions with homemade batch reactor with 40-W 370-nm Kessil lamp; yields were determined by quantitative NMR (supplementary materials section S5.1). §Experiments run as single objective with the objective function to increase yield. Res. time, residence time.

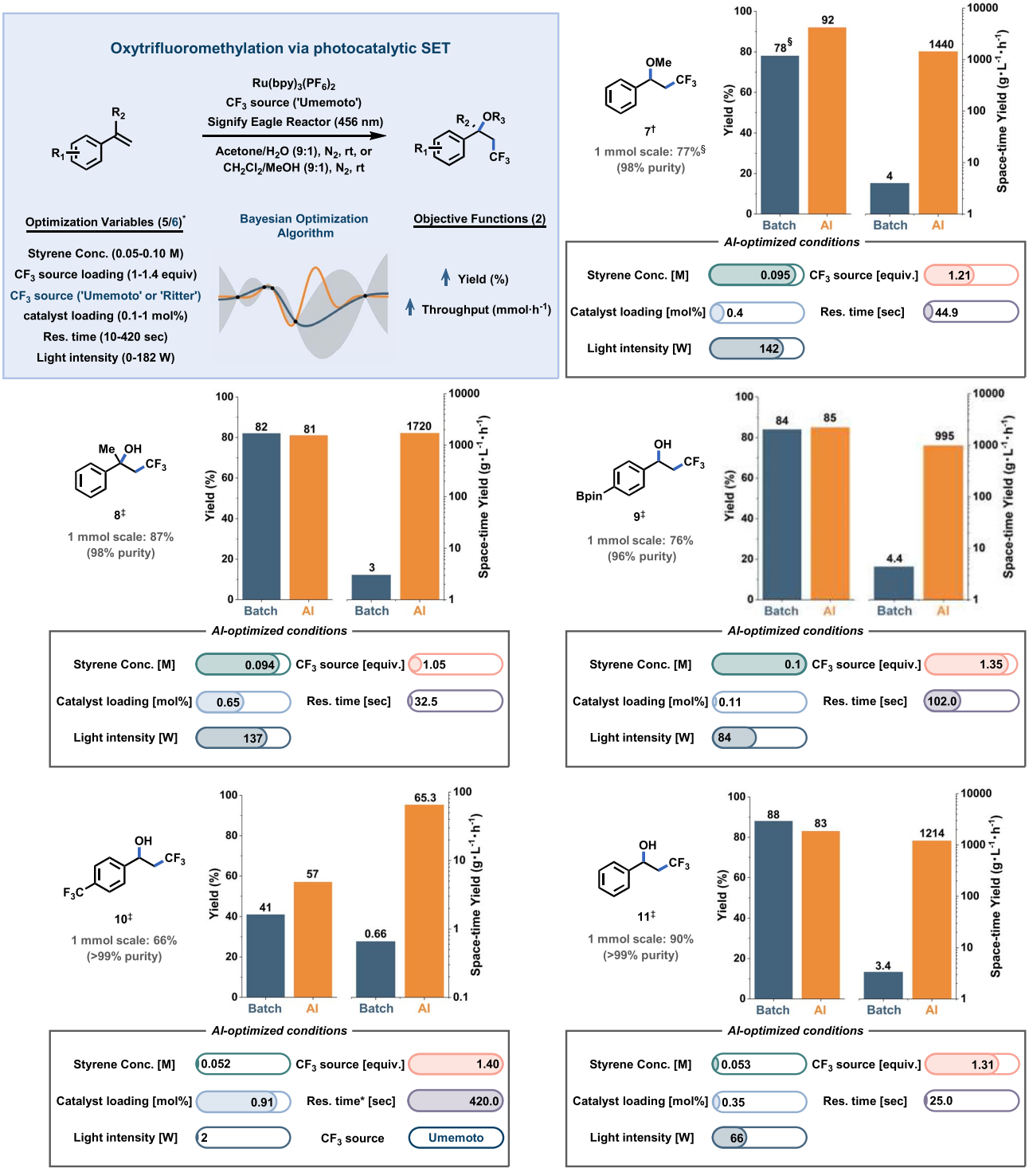

Fig. 5. Substrate scope and associated summary for the three-component oxytrifluoromethylation of alkenes enabled by RoboChem. *Outer bounds of the chemical space explored for all experiments given (for more experimental details and exact chemical spaces explored for each experiment, see supplementary materials section S6.2). †Yield and space-time yield comparisons made directly from the literature. Conditions: Styrene conc. (0.05 M), *fac*-Ir(ppy)$_3$ loading (0.5 mol%), Umemoto loading (1.05 equiv), CH_2Cl_2:MeOH (9:1), 425-nm blue LED (3 W), 2.5 hours. ‡Yield comparisons made directly from the literature. Conditions: Styrene conc. (0.05M), *fac*-Ir(ppy)$_3$ loading (0.5 mol%), Umemoto loading (1.1 equiv), acetone:H_2O (9:1), 425-nm blue LED (3 W), 2 to 4 hours. §Yield > 95% by quantitative NMR.

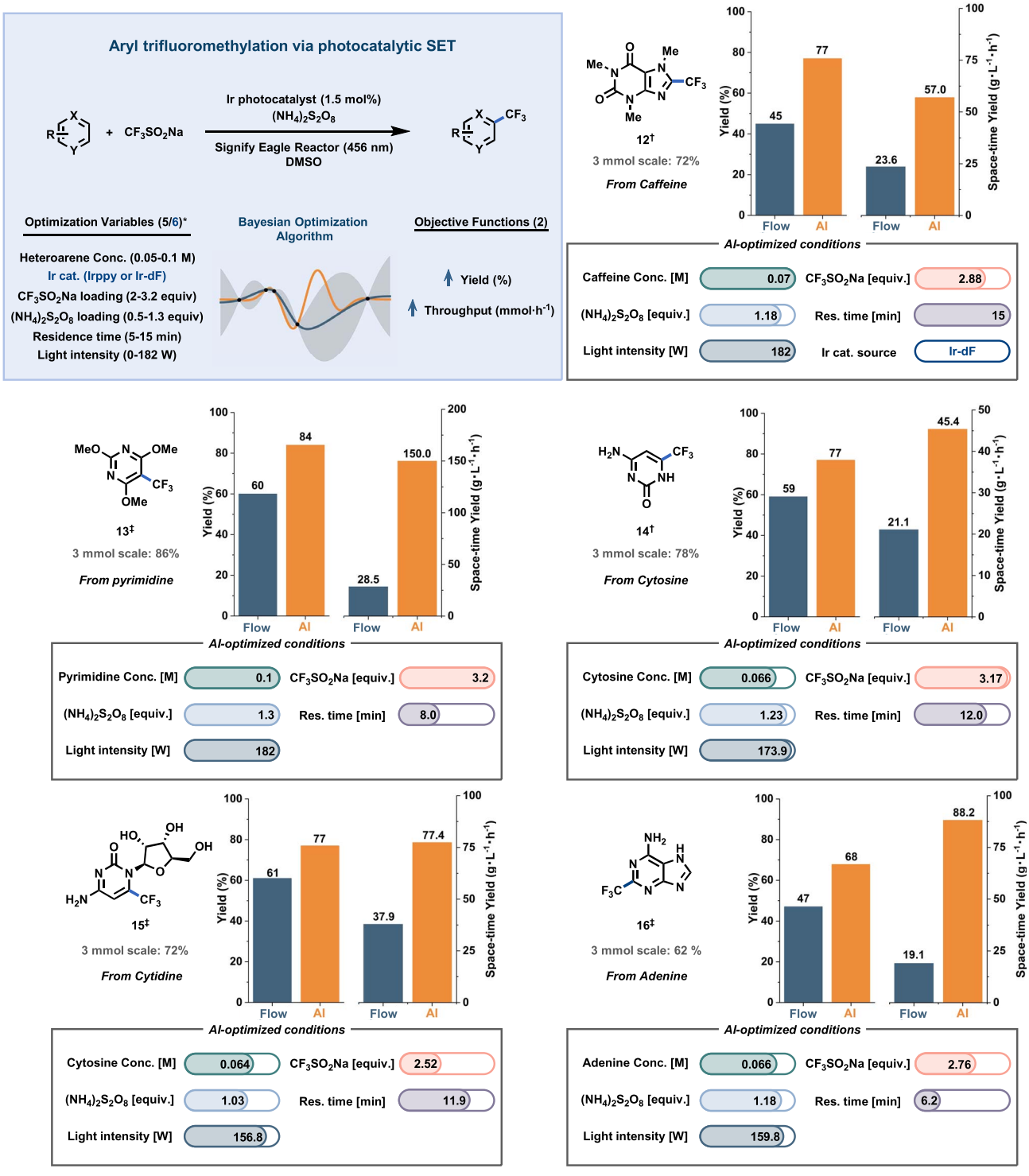

Fig. 6. Substrate scope and associated summary for aryl trifluoromethylation through single electron transfer enabled by RoboChem. *Outer bounds of the chemical space explored for all experiments given (for more experimental details and exact chemical spaces explored for each experiment, see supplementary materials section S7.3). †Yield comparisons made directly from the literature. Conditions: Heteroarene conc. (0.1 M), Ir-dF, $\{Ir[dF(CF_3)ppy]_2\}(dtbpy)]PF_6$ (1 mol%), CF_3SO_2Na equiv. (3 equiv.), $(NH_4)_2S_2O_8$ equiv. (1 equiv.), residence time (30 min), Vapourtec reactor (456 nm, 60 W). ‡Yield and space-time yield comparisons made to reaction carried out by us under literature conditions with Vapourtec Photoreactor (456 nm, 60 W); yields were determined by quantitative NMR (supplementary materials section S7.2).

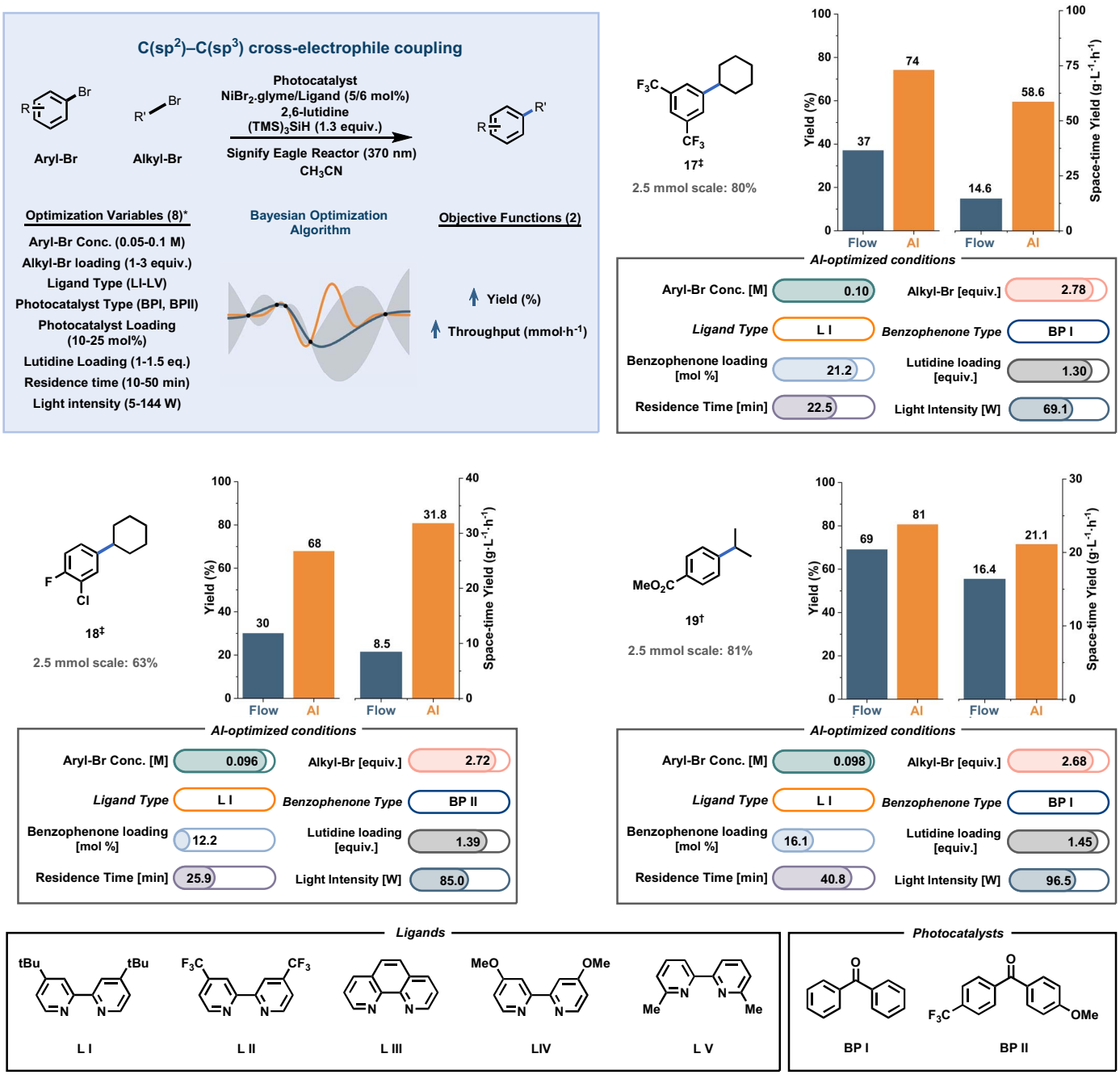

Fig. 7. Substrate scope and associated summary for C(sp^2)–C(sp^3) cross-electrophile coupling enabled by RoboChem. *Outer bounds of the chemical space explored for all experiments given (for more experimental details and exact chemical spaces explored for each experiment, see supplementary materials section S8.3). †Yield comparisons made directly from the literature. Conditions: Aryl bromide conc. (0.1 M), Alkyl bromide (2.5 equiv.), BP II (20 mol%), $NiBr_2$·dtbbp (5 mol%), 2,6-lutidine (1.1 equiv.), $(TMS)_3SiH$ (1.5 equiv.), residence time (45 min), Vapourtec reactor (456 nm, 16 W). ‡Yield and space-time yield comparisons made to reaction carried out by us in duplicate under literature conditions with Vapourtec UV 150 Photoreactor (456 nm, 16 W); yield was determined by quantitative NMR (supplementary materials section S8.2).

match the absorption maximum of the $Ru(bpy)_3$ photocatalyst. Owing to the short residence times, which were as low as 10 s, the internal volume of the photoreactor had to be reduced to 0.26 mL. This adjustment was necessary because at very low residence times (10 s) with a larger internal volume (>3 ml), the syringe pumps struggled to cope with the increased pressure drop across the platform.

The RoboChem platform successfully performed reaction optimization, resulting in conditions that produced outcomes closely aligned with those of the model batch reactions. A significant increase in space-time yield of up to 565-fold was achieved, demonstrating substantial potential for scale-up in the flow reactor. During the scale-up process, a slight improvement in yield was observed compared with that of the optimization carried out on the platform. This can be attributed to the fact that, for scale-up, the internal volume of the reactor was multiplied by a factor of six, whereas the residence time remained the same. Consequently, an associated sixfold increase in flow rate was necessary to maintain the desired residence time, leading to improved mass transfer facilitated by a higher Reynolds number. This

phenomenon accounts for the observed increase in yield compared with that of the platform conditions.

The results indicate a significant dependence of this chemistry on the sustained power applied during the reaction, with higher-power or longer residence time conditions resulting in noticeably lower yields due to photon-induced product degradation. Remarkably, one reaction condition exhibited optimal performance at the lowest "turned-on" power output; specifically, molecule **9** at 2-W optical output. Notably, the choice of the lowest light intensity, particularly when contrasted with the high light intensity used in other examples, further highlights the challenging nature of prediction in this context. Additionally, during the optimization of molecule **9**, various CF_3 sources were screened, including trifluoromethyl thianthrenium triflate (*39*) and Umemoto's reagent, serving as a test case to evaluate discrete variables. The algorithm determined that Umemoto's reagent was the optimal choice for this transformation.

Multiobjective optimization of aryl trifluoromethylation

To provide another example, our objective was to optimize the visible-light photocatalytic trifluoromethylation of highly functionalized heteroarenes developed by our group and researchers from Janssen pharmaceuticals (Fig. 6) (*40*). In our original report, the reaction was carried out in a commercially available Vapourtec UV-150 flow reactor. In the flow photomicroreactor equipped with blue LEDs, we scanned a search space consisting of five reaction parameters (heteroarene concentration, CF_3SO_2Na loading, oxidant loading, residence time, and light intensity), targeting two objective functions [yield (%) and throughput (mmol h^{-1})] for optimization. During the optimization of caffeine trifluoromethylation, we also incorporated a categorical variable to screen for the appropriate photocatalyst. This highlights the capability of the RoboChem platform to evaluate and optimize both discrete and continuous variables. For each substrate, a total of 17 to 35 experiments (including six initialization steps) were conducted within an 11- to 24-hour timeframe.

In this specific example, the RoboChem platform focused on optimizing a diverse range of densely functionalized substrates that hold major interest in drug discovery programs (Fig. 6). Despite the original work being conducted in a flow system, we observed a substantial enhancement in both yield and productivity. This improvement can be attributed to the platform's capacity to tailor the reaction conditions to each substrate individually, coupled with the use of a more potent light source in the flow photomicroreactor. It is well-recognized that increasing the light intensity can inherently influence performance, particularly in the realm of photochemistry (*41*). However, if this transition were the primary factor in enhanced performance, rather than the AI optimization, we would expect to see more uniformity in the optimized conditions across all literature-to-RoboChem transitions. Contrary to this, our findings demonstrate notable variability in these conditions, suggesting a significant and distinct contribution from AI refinement.

Multiobjective optimization of $C(sp^2)$–$C(sp^3)$ cross-electrophile coupling

In our final case study, we focused on optimizing complex photocatalytic transformations that use synergistic catalytic cycles, such as metallaphotocatalysis. The union between photocatalysis and transition-metal catalysis offers distinct reactivity, facilitating otherwise difficult bond formations (*42*). We prioritized carbon-carbon bond formation because of its importance in the pharmaceutical and agrochemical sectors. Specifically, we studied the cross-electrophile coupling of alkyl and aryl bromides to achieve $C(sp^2)$–$C(sp^3)$ bond formation (*43*). Mechanistic insights revealed that the reaction requires a combination of benzophenone HAT photocatalysis, silyl radical–induced halogen atom transfer, and nickel-catalyzed cross-coupling. (*44*, *45*) Given the vast potential chemical space and the delicate balance between the three catalytic cycles, we believed that identifying the optimum would be a serious hurdle for chemists, making it an apt test for the RoboChem platform. In our optimization campaign (Fig. 7), eight reaction parameters were concurrently adjusted: aryl halide concentration, alkyl halide loading, selection among five nickel ligand sources (**L I** to **L V**), choice between two benzophenone photocatalysts (**BP I** and **BP II**), benzophenone and 2,6-lutidine loadings, residence time, and light intensity. We optimized two objective functions: yield (%) and throughput (mmol h^{-1}). For every substrate, either 45 or 60 experiments were conducted, with total optimization durations ranging from 41 to 58 hours. Each experimental phase comprised an initial 20 runs, followed by 25 or 40 runs for optimization.

Initially, we sought to enhance the yield of a substrate that underperformed under literature conditions (*45*). After 60 experiments spanning 58 hours with RoboChem, we successfully elevated the yield of compound **17** from 37 to 77%. Analysis of the data pinpointed the choice of ligand as an important variable. **L V** was suboptimal, likely owing to the steric interference of its two methyl groups, highlighting the sensitivity of the nickel catalytic cycle toward steric hindrance. **L II**, **L III**, and **L IV** performed adequately but were outperformed by **L I**. This observation was swiftly recognized by the algorithm, which selected **L I** in 31 of the 40 optimization runs. **BP I** emerged as the preferred HAT catalyst, despite underwhelming results under literature conditions when compared with **BP II** (*45*). Moreover, higher light intensities, considered detrimental in literature model reactions (*45*), proved beneficial.

Subsequently, we undertook optimization for compounds **18** and **19**. Both endeavors yielded valuable datasets with both positive and negative results (detailed in supplementary materials), which led ultimately to tailored reaction conditions, including the selection of HAT catalyst **BP II** for compound **18**, that substantially improved yields. This result underscores the potential pitfalls of optimizing OFAT on a model substrate, which may inadvertently narrow the chemistry to that molecule, limiting broader applicability. As in prior case studies, our NMR yields closely mirrored isolated yields, underscoring our platform's precision and reproducibility. This also highlights the benefit of using flow technology to control mass, heat, and photon transport across varied reaction scales (*6*), an advantage not available with analogous automated batch reactor systems.

Conclusions and outlook

As shown in this work, RoboChem constitutes a versatile robotic platform for the self-optimization, intensification, and/or scale-up of a diverse set of photocatalytic reactions. Operated through a BO algorithm, this platform is able to explore the presented parameter space, ultimately furnishing customized reaction conditions attuned to the specific needs of each substrate. By substantially reducing the need for human intervention, RoboChem not only increases operational safety but also liberates researchers to dedicate more time to the more creative aspects of chemistry, thereby freeing them from the drudgery of reaction optimization and intensification tasks.

The modularity of the robotic platform is an asset of our design, and we foresee its integration with different types of flow reactors and process analytical technologies in the future. Moreover, by individually optimizing reaction parameters and generating datasets that include both optimal and suboptimal conditions, intricate relationships between the targeted reaction parameters, the substrate structures, and the objective functions can be uncovered. The ability to automatically generate rich datasets, obtained within a highly reproducible reactor environment, can contribute to the future digitization of synthetic chemistry.

Methods summary

For a more detailed description of the preparation and running of the platform, and

generation of stock solutions, see the supplementary materials. A short summary is provided below.

Analytics preparation

A calibration curve was established for the benchtop NMR by using a reference standard featuring a molecule within a comparable parts-per-million range as the peaks of interest in the product (e.g., α,α,α-trifluorotoluene for the photocatalytic oxytrifluoromethylation and the aryl trifluoromethylation). These calibration measurements were conducted under the exact NMR conditions as those used during the campaign. Subsequently, a scripting file was generated to automate the processing of the product's NMR spectrum. Additionally, the NMR instrument underwent shimming procedures in preparation for the campaign's commencement.

User input

The experiment was then initialized by using the GUI to input the settings for the optimization campaign (chemical space, stock solution concentrations, NMR settings, scripting file, etc.).

Platform operation

Stock solutions were prepared according to the procedures detailed in the supplementary materials. The solutions were subsequently transferred to 4-ml glass vials and then loaded into the liquid handler. From the GUI, the system was then run. The liquid handler makes up the reaction solution which was automatically introduced into the continuous-flow photochemical reactor. Upon exiting the reactor, the reaction slug was analyzed by benchtop NMR, and subsequently, the objective function (yield or throughput) was calculated. This information was sent back to the BO algorithm, which defines the next set of conditions. Every campaign kicks off with a Latin Hypercube sampling initialization, after which optimization toward maximizing the objective function happens. The optimization cycle was stopped by the operator after the hypervolume appeared to reach a maximum or when the total amount of runs indicated at the outset was realized. During the optimization campaign, the remaining amount of stock solutions and carrier solvent were checked periodically and refilled if necessary. If the stock solutions are not refilled in time, the platform will automatically stop the sequence until refilling.

REFERENCES AND NOTES

1. M. H. Shaw, J. Twilton, D. W. C. MacMillan, Photoredox Catalysis in Organic Chemistry. *J. Org. Chem.* **81**, 6898–6926 (2016). doi: 10.1021/acs.joc.6b01449; pmid: 27477076
2. K. L. Skubi, T. R. Blum, T. P. Yoon, Dual Catalysis Strategies in Photochemical Synthesis. *Chem. Rev.* **116**, 10035–10074 (2016). doi: 10.1021/acs.chemrev.6b00018; pmid: 27109441
3. T. Noël, E. Zysman-Colman, The promise and pitfalls of photocatalysis for organic synthesis. *Chem Catal.* **2**, 468–476 (2022). doi: 10.1016/j.checat.2021.12.015
4. D. M. Arias-Rotondo, J. K. McCusker, The photophysics of photoredox catalysis: A roadmap for catalyst design. *Chem. Soc. Rev.* **45**, 5803–5820 (2016). doi: 10.1039/C6CS00526H; pmid: 27711624
5. C. J. Taylor *et al*., A Brief Introduction to Chemical Reaction Optimization. *Chem. Rev.* **123**, 3089–3126 (2023). doi: 10.1021/acs.chemrev.2c00798; pmid: 36820880
6. S. D. A. Zondag, D. Mazzarella, T. Noël, Scale-Up of Photochemical Reactions: Transitioning from Lab Scale to Industrial Production. *Annu. Rev. Chem. Biomol. Eng.* **14**, 283–300 (2023). doi: 10.1146/annurev-chembioeng-101121-074313; pmid: 36913716
7. K. C. Harper *et al*., Commercial-Scale Visible Light Trifluoromethylation of 2-Chlorothiophenol Using CF_3I Gas. *Org. Process Res. Dev.* **26**, 404–412 (2022). doi: 10.1021/acs.oprd.1c00436
8. C. Bottecchia *et al*., Manufacturing Process Development for Belzutifan, Part 2: A Continuous Flow Visible-Light-Induced Benzylic Bromination. *Org. Process Res. Dev.* **26**, 516–524 (2022). doi: 10.1021/acs.oprd.1c00240
9. T. Van Gerven, G. Mul, J. Moulijn, A. Stankiewicz, A review of intensification of photocatalytic processes. *Chem. Eng. Process.* **46**, 781–789 (2007). doi: 10.1016/j.cep.2007.05.012
10. L. Buglioni, F. Raymenants, A. Slattery, S. D. A. Zondag, T. Noël, Technological Innovations in Photochemistry for Organic Synthesis: Flow Chemistry, High-Throughput Experimentation, Scale-up, and Photoelectrochemistry. *Chem. Rev.* **122**, 2752–2906 (2022). doi: 10.1021/acs.chemrev.1c00332; pmid: 34375082
11. D. Cambié, C. Bottecchia, N. J. W. Straathof, V. Hessel, T. Noël, Applications of Continuous-Flow Photochemistry in Organic Synthesis, Material Science, and Water Treatment. *Chem. Rev.* **116**, 10276–10341 (2016). doi: 10.1021/acs.chemrev.5b00707; pmid: 26935706
12. J. Freiesleben, J. Keim, M. Grutsch, Machine learning and Design of Experiments: Alternative approaches or complementary methodologies for quality improvement? *Qual. Reliab. Eng. Int.* **36**, 1837–1848 (2020). doi: 10.1002/qre.2579
13. M. I. Jordan, T. M. Mitchell, Machine learning: Trends, perspectives, and prospects. *Science* **349**, 255–260 (2015). doi: 10.1126/science.aaa8415; pmid: 26185243
14. C. Houben, A. A. Lapkin, Automatic discovery and optimization of chemical processes. *Curr. Opin. Chem. Eng.* **9**, 1–7 (2015). doi: 10.1016/j.coche.2015.07.001
15. F. Häse, L. M. Roch, A. Aspuru-Guzik, Chimera: Enabling hierarchy based multi-objective optimization for self-driving laboratories. *Chem. Sci.* **9**, 7642–7655 (2018). doi: 10.1039/C8SC02239A; pmid: 30393525
16. A. D. Clayton *et al*., Bayesian Self-Optimization for Telescoped Continuous Flow Synthesis. *Angew. Chem. Int. Ed.* **62**, e202214511 (2023). doi: 10.1002/anie.202214511; pmid: 36346840
17. B. J. Shields *et al*., Bayesian reaction optimization as a tool for chemical synthesis. *Nature* **590**, 89–96 (2021). doi: 10.1038/s41586-021-03213-y; pmid: 33536653
18. D. Perera *et al*., A platform for automated nanomole-scale reaction screening and micromole-scale synthesis in flow. *Science* **359**, 429–434 (2018). doi: 10.1126/science.aap9112; pmid: 29371464
19. H. W. Hsieh, C. W. Coley, L. M. Baumgartner, K. F. Jensen, R. I. Robinson, Photoredox Iridium-Nickel Dual-Catalyzed Decarboxylative Arylation Cross-Coupling: From Batch to Continuous Flow via Self-Optimizing Segmented Flow Reactor. *Org. Process Res. Dev.* **22**, 542–550 (2018). doi: 10.1021/acs.oprd.8b00018
20. C. Avila *et al*., Automated stopped-flow library synthesis for rapid optimisation and machine learning directed experimentation. *Chem. Sci.* **13**, 12087–12099 (2022). doi: 10.1039/D2SC03016K; pmid: 36349112
21. C. P. Breen, A. M. K. Nambiar, T. F. Jamison, K. F. Jensen, Ready, Set, Flow! Automated Continuous Synthesis and Optimization. *Trends Chem.* **3**, 373–386 (2021). doi: 10.1016/j.trechm.2021.02.005
22. K. Kandasamy *et al*., Tuning Hyperparameters without Grad Students: Scalable and Robust Bayesian Optimisation with Dragonfly. *J. Mach. Learn. Res.* **21**, 1–27 (2020).
23. T. Wan *et al*., Accelerated and Scalable $C(sp^3)$-H Amination via Decatungstate Photocatalysis Using a Flow Photoreactor Equipped with High-Intensity LEDs. *ACS Cent. Sci.* **8**, 51–56 (2022). doi: 10.1021/acscentsci.1c01109; pmid: 35106372
24. Noel Research Group, Robochem, v1, Zenodo (2023); https://doi.org/10.5281/zenodo.10261472.
25. B. Shahriari, K. Swersky, Z. Wang, R. P. Adams, N. de Freitas, Taking the Human Out of the Loop: A Review of Bayesian Optimization. *Proc. IEEE* **104**, 148–175 (2016). doi: 10.1109/JPROC.2015.2494218
26. A. M. K. Nambiar *et al*., Bayesian Optimization of Computer-Proposed Multistep Synthetic Routes on an Automated Robotic Flow Platform. *ACS Cent. Sci.* **8**, 825–836 (2022). doi: 10.1021/acscentsci.2c00207; pmid: 35756374
27. W. Li, L. Lu, X. Xie, M. Yang, A novel extension algorithm for optimized Latin hypercube sampling. *J. Stat. Comput. Simul.* **87**, 2549–2559 (2017). doi: 10.1080/00949655.2017.1340475
28. M. D. McKay, R. J. Beckman, W. J. Conover, Comparison of Three Methods for Selecting Values of Input Variables in the Analysis of Output from a Computer Code. *Technometrics* **21**, 239–245 (1979).
29. A. D. Clayton *et al*., Algorithms for the self-optimisation of chemical reactions. *React. Chem. Eng.* **4**, 1545–1554 (2019). doi: 10.1039/C9RE00209J
30. S. Daulton, M. Balandat, E. Bakshy, Differentiable Expected Hypervolume Improvement for Parallel Multi-Objective Bayesian Optimization. arXiv:2006.05078 [stat.ML] (2020).
31. S. Steiner *et al*., Organic synthesis in a modular robotic system driven by a chemical programming language. *Science* **363**, eaav2211 (2019). doi: 10.1126/science.aav2211; pmid: 30498165
32. S. V. Ley, D. E. Fitzpatrick, R. J. Ingham, R. M. Myers, Organic synthesis: March of the machines. *Angew. Chem. Int. Ed.* **54**, 3449–3464 (2015). doi: 10.1002/anie.201410744; pmid: 25586940
33. Noel Research Group, Robochem Datasets, v1, Zenodo (2023); https://doi.org/10.5281/zenodo.10262296.
34. M. D. Wilkinson *et al*., The FAIR Guiding Principles for scientific data management and stewardship. *Sci. Data* **3**, 160018 (2016). doi: 10.1038/sdata.2016.18; pmid: 26978244
35. M. P. Maloney *et al*., Negative Data in Data Sets for Machine Learning Training. *J. Org. Chem.* **88**, 5239–5241 (2023). doi: 10.1021/acs.joc.3c00844; pmid: 37126471
36. Z. Wen *et al*., Optimization of a Decatungstate-Catalyzed $C(sp^3)$-H Alkylation Using a Continuous Oscillatory Millistructured Photoreactor. *Org. Process Res. Dev.* **24**, 2356–2361 (2020). doi: 10.1021/acs.oprd.0c00235; pmid: 33100815
37. T. E. Schirmer, A. B. Rolka, T. A. Karl, F. Holzhausen, B. König, Photocatalytic C-H Trifluoromethylthiolation by the Decatungstate Anion. *Org. Lett.* **23**, 5729–5733 (2021). doi: 10.1021/acs.orglett.1c01870; pmid: 34260256
38. Y. Yasu, T. Koike, M. Akita, Three-component oxytrifluoromethylation of alkenes: Highly efficient and regioselective difunctionalization of C=C bonds mediated by photoredox catalysts. *Angew. Chem. Int. Ed.* **51**, 9567–9571 (2012). doi: 10.1002/anie.201205071; pmid: 22936394
39. H. Jia, A. P. Häring, F. Berger, L. Zhang, T. Ritter, Trifluoromethyl Thianthrenium Triflate: A Readily Available Trifluoromethylating Reagent with Formal CF_3^+, $CF_3^•$, and CF_3^- Reactivity. *J. Am. Chem. Soc.* **143**, 7623–7628 (2021). doi: 10.1021/jacs.1c02606; pmid: 33985330
40. I. Abdiaj, C. Bottecchia, J. Alcazar, T. Noël, Visible-Light-Induced Trifluoromethylation of Highly Functionalized Arenes and Heteroarenes in Continuous Flow. *Synthesis (Stuttg.)* **49**, 4978–4985 (2017). doi: 10.1055/s-0036-1588527
41. T. D. Svejstrup *et al*., Effects of Light Intensity and Reaction Temperature on Photoreactions in Commercial Photoreactors. *ChemPhotoChem* **5**, 808–814 (2021). doi: 10.1002/cptc.202100059
42. A. Y. Chan *et al*., Metallaphotoredox: The Merger of Photoredox and Transition Metal Catalysis. *Chem. Rev.* **122**, 1485–1542 (2022). doi: 10.1021/acs.chemrev.1c00383; pmid: 34793128
43. D. A. Everson, D. J. Weix, Cross-electrophile coupling: Principles of reactivity and selectivity. *J. Org. Chem.* **79**, 4793–4798 (2014). doi: 10.1021/jo500507s; pmid: 24820397
44. P. Zhang, C. C. Le, D. W. C. MacMillan, Silyl Radical Activation of Alkyl Halides in Metallaphotoredox Catalysis: A Unique Pathway for Cross-Electrophile Coupling. *J. Am. Chem. Soc.* **138**, 8084–8087 (2016). doi: 10.1021/jacs.6b04818; pmid: 27263662
45. A. Luridiana *et al*., The Merger of Benzophenone HAT Photocatalysis and Silyl Radical-Induced XAT Enables Both Nickel-Catalyzed Cross-Electrophile Coupling and 1,2-Dicarbofunctionalization of Olefins. *ACS Catal.* **12**, 11216–11225 (2022). doi: 10.1021/acscatal.2c03805; pmid: 36158902

ACKNOWLEDGMENTS

Funding: We gratefully acknowledge the generous funding provided by the Dutch Research Council (NWO) under the Open Technology Program (Multi-Modal Photochemistry, no. 18433) (A.S., D.P., and T.N.). Z.W. was supported by the China Scholarship Council (CSC, no. 201808440313). Furthermore, we extend our gratitude for the generous funding received from the European Union H2020 research and innovation program under the

European Research Council program (FlowHAT, no. 101044355) (T.N.), Marie S. Curie Grant Agreement (PhotoReAct, no. 956324) (P.T. and T.N.), and MSCA Individual Fellowship program (SELECTFLOW, no. 101061835) (J.S.O.). **Author contributions:** A.S., Z.W., and D.P. developed, assembled and maintained the hardware of the robotic platform; A.S., Z.W., P.T., and D.P. developed the code of the controller that steered the robotic platform; P.T. implemented and assessed the BO algorithm; A.S., Z.W., J.S.O., T.d.H., and T.N. selected and supervised the chemistry to be run on the robotic platform; A.S., Z.W., and J.S.O. made the stock solutions, evaluated the reaction progress, and carried out the product isolation; P.T. implemented the GUI; A.S., P.T., and T.N. drafted the manuscript with input from all authors; and T.N. conceived the idea for this work and secured the funding. **Competing interests:** The authors declare no competing interests. **Data and materials availability:** All the code for the automated platform is available at https://github.com/Noel-Research-Group/Robochem_v1.0. An archived version of the code is available on Zenodo (*24*). Tabulated data are also available on Zenodo (*33*).

SUPPLEMENTARY MATERIALS

science.org/doi/10.1126/science.adj1817
Materials and Methods
Figs. S1 to S120
Tables S1 to S57
NMR Spectra
References (*46*–*50*)

Submitted 11 June 2023; resubmitted 12 October 2023
Accepted 13 December 2023
10.1126/science.adj1817